Histidine 61: An Important Heme Ligand in the Soluble Fumarate Reductase from *Shewanella frigidimarina*[†,‡]

Emma L. Rothery,[§] Christopher G. Mowat,[§,||] Caroline S. Miles,[||] Malcolm D. Walkinshaw,[||] Graeme A. Reid,[||] and Stephen K. Chapman*[,§]

School of Chemistry, University of Edinburgh, West Mains Road, Edinburgh EH9 3JJ, U.K., and Institute of Cell and Molecular Biology, University of Edinburgh, Mayfield Road, Edinburgh EH9 3JR, U.K.

Received June 26, 2003; Revised Manuscript Received September 4, 2003

ABSTRACT: An examination of the X-ray structure of the soluble fumarate reductase from *Shewanella frigidimarina* [Taylor, P., Pealing, S. L., Reid, G. A., Chapman, S. K., and Walkinshaw, M. D. (1999) *Nat. Struct. Biol. 6,* 1108−1112] shows the presence of four, bis-His-ligated, *c*-type hemes and one flavin adenine dinucleotide, FAD. The heme groups provide a "molecular wire" for the delivery of electrons to the FAD. Heme IV is closest to the FAD (7.4 Å from heme methyl to FAD C7), and His61, a ligand to heme IV, is also close (8.4 Å to FAD C7). Electron delivery to the FAD from the heme groups must proceed via heme IV, as hemes I−III are too far from the FAD for feasible electron transfer. To examine the importance of heme IV and its ligation for enzyme function, we have substituted His61 with both methionine and alanine. Here we describe the crystallographic, kinetic, and electrochemical characterization of the H61M and H61A mutant forms of the *Shewanella* fumarate reductase. The crystal structures of these mutant forms of the enzyme have been determined to 2.1 and 2.2 Å resolution, respectively. Substitution of His61 with alanine results in heme IV having only one protein ligand (His86), the sixth coordination position being occupied by an acetate ion derived from the crystal cryoprotectant solution. In the structure of the H61M enzyme, Met61 is found not to ligate the heme iron, a role that is taken by a water molecule. Apart from these features, there are no significant structural alterations as a result of either substitution. Both the H61M-Fcc_3 and H61A-Fcc_3 mutant enzymes are catalytically active but exhibit marked decreases in the value of k_{cat} for fumarate reduction with respect to that of the wild type (5- and 10-fold lower, respectively). There is also a significant shift in the pK_a values for the mutant enzymes, from 7.5 for the wild type to 8.26 for H61M and 9.29 for H61A. The fumarate reductase activity of both mutant enzymes can be recovered to ∼80% of that seen for the wild type by the addition of exogenous imidazole. In the case of H61A, recovery of activity is also accompanied by a shift of the pK_a from 9.29 to 7.46 (close, and within experimental error, to that for the wild type). Pre-steady-state kinetic measurements show clearly that rate constants for the fumarate dependent reoxidation of the heme groups are adversely affected by the mutations. The solvent isotope effect for fumarate reduction in the wild-type enzyme has a value of 8.0, indicating that proton delivery is substantially rate limiting. This value falls to 5.6 and 2.2 for the H61M and H61A mutants, respectively, indicating that electron transfer, rather than proton transfer, is becoming more rate-limiting in the mutant enzymes.

Many bacteria contain fumarate reductases, which enable them to utilize fumarate as a terminal electron acceptor for respiration. Most fumarate reductases are bound to the inner face of the cytoplasmic membrane, contain both iron−sulfur centers and FAD[1] (*1*, *2*), and are closely related to the succinate dehydrogenases. In *Shewanella* species, however, a soluble, periplasmic, fumarate reductase is produced. The *Shewanella* enzyme contains four *c*-type heme groups (all of which are bis-His-ligated) and one FAD, and has been designated as flavocytochrome c_3 (Fcc_3) (*3*). A number of crystal structures of Fcc_3 from *Shewanella* species are now available [PDB entries 1QJD (*4*), 1D4E (*5*), and 1QO8 (*6*)]. These Fcc_3 structures show that the region around the FAD (the site of fumarate reduction) is essentially the same as that seen in the membrane-bound fumarate reductases from *Escherichia coli* (*1*) and *Wolinella succinogenes* (*7*, *8*). This conservation of active site structure has been used as

[†] This work was supported by the UK Biotechnology and Biological Sciences Research Council (BBSRC) and by the Wellcome Trust-funded Edinburgh Protein Interaction Centre (EPIC). E.L.R. acknowledges studentship funding from EPSRC. Synchrotron access at EMBL Hamburg was supported by the European Community-Access to Research Infrastructure Action of the Improving Human Potential Programme to the EMBL Hamburg Outstation (Contract HPRI-CT-1999-00017).

[‡] The atomic coordinates have been deposited in the Protein Data Bank as entries 1P2H (H61M) and 1P2E (H61A).

* To whom correspondence should be addressed: School of Chemistry, University of Edinburgh, West Mains Road, Edinburgh EH9 3JJ, U.K. E-mail: S.K.Chapman@ed.ac.uk. Fax or phone: (44) 131 650 4760.

[§] School of Chemistry, University of Edinburgh.

[||] Institute of Cell and Molecular Biology, University of Edinburgh.

[1] Abbreviations: Fcc_3, flavocytochrome c_3; H61A, histidine61 → alanine mutation; H61M, histidine61 → methionine mutation; FAD, flavin adenine dinucleotide; pL, equivalent of pH in mixed isotope solvents.

10.1021/bi030159z CCC: $25.00
Published on Web 10/25/2003

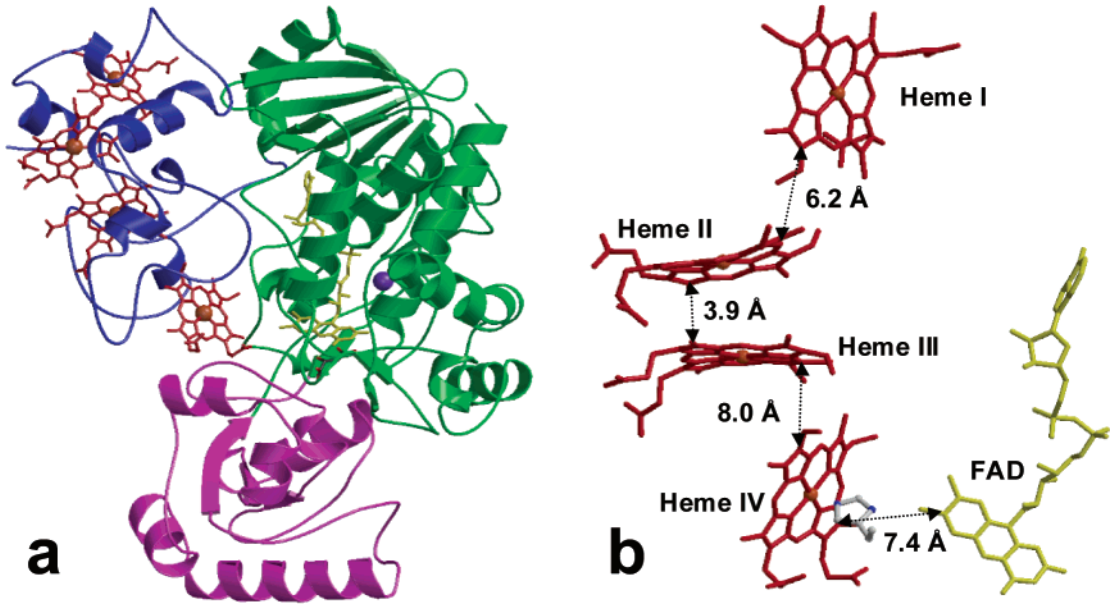

FIGURE 1: Structure of Fcc_3. The three domains are color-coded: heme domain in blue, flavin domain in green, and clamp domain in magenta. The positions of the redox cofactors are clearly shown as is the degree of solvent exposure of the heme groups. This figure was generated using BOBSCRIPT (*33*) and RASTER3D (*34*).

evidence for a universal mechanism for fumarate reduction in all these enzymes (*4*). The details of this mechanism, which involves hydride transfer from FAD N5 to substrate C2 and proton transfer from Arg402 to substrate C3, have been confirmed in a series of recent studies (*9*−*14*).

The structure of Fcc_3 from *Shewanella frigidimarina* (*4*) is shown in Figure 1a. It is clear that three of the heme groups (hemes I−III) are reasonably well exposed and as such are ideal for accepting electrons from the electron donor, which is believed to be the membrane-bound tetraheme cytochrome, CymA (*15*, *30*). Heme IV, on the other hand, is more buried and is close to the FAD. Clearly, electrons being passed to the FAD must travel via heme IV. All of the redox cofactors are close together, with the shortest edge-to-edge distance being 3.9 Å between hemes II and III and the longest being 8.0 Å between hemes III and IV (Figure 1b) (*4*). These short distances are ideal for fast electron transfer. Indeed, protein film voltammetry experiments have shown that electron transfer through the hemes to the FAD is indeed fast and cannot be rate-limiting (*16*). An alternative idea is that proton transfer to the active site acid is rate-limiting, and such a proton transfer pathway has already been proposed (*9*−*11*).

To gain further insight into electron transfer in Fcc_3, we have investigated the effect of changing the ligation of the iron in heme IV. In the paper presented here, we report our results on the effects of substituting His61 with either methionine or alanine. We describe the kinetic and electrochemical characterizations of the H61M-Fcc_3 and H61A-Fcc_3 mutant enzymes together with their high-resolution X-ray crystal structures.

MATERIALS AND METHODS

DNA Manipulation, Strains, Media, and Growth. The mutant enzyme H61A-Fcc_3 was generated by site-directed mutagenesis using the method of Kunkel and Roberts (*17*) as described previously (*3*, *9*). The mutagenic oligonucleotide CTCATGCTTCTGCTTTCCCTGGCG (which substitutes histidine with alanine) was used. Mismatched bases are underlined. The modified coding sequence was cloned into the broad-host range expression plasmid pMMB503EH (*18*) on an ~1.8 kb *Eco*RI−*Hin*dIII fragment to generate pCM122 (H61A *fccA*/pMMB503EH).

The mutant enzyme H61M-Fcc_3 was generated using the QuikChange XL Site-Directed Mutagenesis Kit (Stratagene). The template for the reaction was pEGX1 (*fccA*/pMMB503EH) (*3*). Oligonucleotides were designed to incorporate the histidine 61 to methionine change and were complementary to the same sequence on both strands of the plasmid. The oligonucleotide complementary to the antisense strand is GCTCATGCTTCTATGTTCCCTGGCGAAG, while the oligonucloetide complementary to the sense strand is CTTCGCCAGGGAACATAGAAGCATGAGC. Mismatched bases are underlined. Temperature cycling, product digestion with *Dpn*I, and transformation of *E. coli* XL-10 Gold ultracompetent cells were carried out as described in the Stratagene protocol.

The plasmids that were generated, pCM122 (H61A *fccA*/pMMB503EH) and pCM147 (H61M *fccA*/pMMB503EH), were screened for the required mutations by automated sequencing using an ABI Prism 3100 genetic analyzer, and the mutated *fccA* coding sequences were similarly sequenced to verify that no secondary mutations had been introduced. Expression of both mutant enzymes in Δ*fccA S. frigidimarina* strain EG301 (*3*) was carried out as described previously (*9*).

Protein Purification and Determination of FAD Content. Wild-type and mutant forms of Fcc_3 were purified as previously reported (*19*). Protein samples for crystallization and mass spectrometry were subjected to an additional purification step using FPLC with a 1 mL Resource Q column (Pharmacia) as described by Pealing *et al*. (*20*). Protein concentrations were determined using the Soret band absorption coefficient for the reduced enzyme (752.8 mM^{-1} cm^{-1} at 419 nm) (*19*).

The FAD content of Fcc_3 mutants was determined using the method of Macheroux (*21*), and all steady-state rate

constants were corrected for the percentage of FAD present. Mass spectrometry of proteins was carried out using a Micromass Platform II electrospray mass spectrometer. Samples were prepared in 0.1% (v/v) formic acid before being diluted 1:1 with acetonitrile and introduced into the spectrometer via direct infusion. The spectrometer was standardized using horse heart myoglobin.

Steady-State Kinetics. The steady-state kinetics of fumarate reduction were followed at 25 °C as described by Turner *et al.* (*22*). The fumarate-dependent reoxidation of reduced methyl viologen was monitored at 600 nm using a Shimadzu UV-PC 1501 spectrophotometer. To ensure anaerobicity, the spectrophotometer was housed in a Belle Technology glovebox under a nitrogen atmosphere with the O_2 level kept below 2 ppm. Assay buffers contained 0.45 M NaCl and 0.2 mM methyl viologen and were adjusted to the appropriate pH values using 0.05 M HCl or NaOH as follows: Tris-HCl at pH 7.0−9.0, MES/NaOH at pH 5.4−6.8, and CHES/NaOH at pH 8.6−10. The viologen was reduced by addition of sodium dithionite until a reading of ∼1 absorbance unit was obtained (corresponding to ∼80 μM reduced methyl viologen). The concentration of reduced methyl viologen could be varied between 100 and 20 μM with no effect on the rate of reaction. A known concentration of the enzyme was added and the reaction initiated by addition of fumarate (0−1 mM).

Rescue of activity assays were performed in the manner described above. The enzyme was preincubated with a known concentration of imidazole at 25 °C for several minutes before initiation of the assay by addition of fumarate under saturating conditions. All assays were carried out in 0.05 M Tris-HCl buffer containing 0.45 M NaCl and corrected to pH 7.2.

Kinetic parameters K_m and k_{cat} were determined from the steady-state results using nonlinear regression analysis (Microcal Origin software). pH profiles were constructed by activity measurement under saturating conditions at a range of pH values

Solvent Isotope Effects. The effect on turnover rates upon deuteration of the solvent was studied via the steady-state assay method described above. Buffer and substrate solutions were prepared in both D_2O and H_2O, and the assay was performed under saturating fumarate conditions. DCl or NaOD was titrated into the deuterated buffer to correct the pD as required, applying the equation pD = pH meter reading + 0.4, to correct for the acidity of the pH electrode itself (*23*). The stock protein solution was prepared in H_2O and then concentrated such that the addition of the protonated enzyme solution was less than 0.05% of the total volume of the assay. The percentage of D_2O in the buffer was varied between 0 and 100% by addition of the correct proportion of deuterated and protonated buffer to the assay cuvette. The protein was allowed to equilibrate with the deuterated buffer for ∼30 s before initiation of the assay by addition of fumarate. For assays requiring the presence of imidazole, a stock solution of 2 M imidazole in protonated buffer was prepared. Small aliquots of imidazole were then preincubated with the protein (to give a final imidazole concentration of 5 mM) prior to initiation of the assay under saturating fumarate conditions. The rate constants that were obtained were plotted as a function of the D_2O concentration to construct a proton inventory which was then fitted to a multisite model, as described by Schowen *et al.* (*24*). The solvent isotope effect for each mutation was calculated with the ratio k_H/k_D.

Pre-Steady-State Kinetics. Pre-steady-state kinetic analysis was carried out using an Applied Photophysics SF.17MV stopped-flow spectrophotometer contained in a Belle Technology glovebox, maintained under a nitrogen atmosphere (<2 ppm O_2). The buffer was Tris-HCl (as used in steady-state experiments) containing 0.45 M NaCl and 0.05 M Tris and adjusted to pH 7.2. All experiments were conducted at 25 °C. The stock enzyme solution was reduced by titration with sodium dithionite, and excess reductant was then removed via gel filtration (Bio-Rad Econo-pac 10DG 10 mL column) within the anaerobic environment. Fumarate was prepared in the same buffer as the stock enzyme, and its concentration was varied from 1 to 500 μM. The course of fumarate-dependent heme oxidation was monitored at 418 nm. Traces that were obtained were fitted to a double-exponential decay, and the rates that were obtained were plotted as a function of the fumarate concentration. All fitting was done using Origin software (Microcal).

Binding of Exogenous Ligands. Aliquots of a solution (3 mL) containing ca. 0.1 μM Fcc_3 buffered in 50 mM Tris-HCl, containing 0.45 M NaCl at pH 7.2, were pipetted into a cuvette, and maintained anaerobically, as described above. Where the reduced enzyme was required, the stock enzyme solution was reduced by titration with sodium dithionite, and excess reductant was then removed via gel filtration (BioRad Econo-pac 10DG 10 mL column) within the anaerobic environment. Aliquots of the concentrated ligand prepared in the same buffer as the enzyme solution were added to the cuvette and the spectra recorded from 350 to 800 nm using a Shimadzu UV-PC 1501 spectrophotometer. Absorbancies were corrected for dilution, and difference spectra were calculated. All spectra were recorded at 25 °C and solutions allowed at least 5 min of equilibration time.

Potentiometric Titrations. Redox titrations were performed using the method of Dutton *et al.* (*25*). A 10 μM Fcc_3 solution was made up in 0.1 M phosphate buffer at 25 °C. For titrations recorded in the presence of imidazole, the stock enzyme was prepared in a 0.1 M phosphate buffer containing 5 mM imidazole. The solution was titrated electrochemically as previously described (*22*) using the soluble mediators (1−5 μM) phenazine methosulfate, 2-hydroxy-1,4-naphthoquinone, FMN, methyl viologen, and benzyl viologen, and using sodium dithionite as the reductant, and potassium ferricyanide as the oxidant. After each addition of oxidant and/or reductant, the solution was allowed 10−15 min of equilibration time. Spectra were recorded on a Shimadzu UV-PC 1501 spectrophotometer. The electrochemical potential of the solution was monitered at 25 °C using a CD740 meter (WPA) coupled to a Pt/calomel electrode (Russell pH Ltd.). All potentials are reported versus the standard hydrogen electrode using the relationship $E_{SHE} = E_{SCE} + 241$ mV. All redox titrations were performed within a Belle Technology glovebox with O_2 levels kept at <3 ppm.

Crystallization and Refinement. Crystallization of H61M and H61A flavocytochromes c_3 was carried out by hanging drop vapor diffusion at 4 °C in Linbro plates. Crystals were obtained with well solutions comprising 100 mM Tris-HCl buffer (pH 7.8−8.5) (measured at 25 °C), 80 mM NaCl, 16−19% PEG 8000, and 10 mM fumarate. Hanging drops (4 μL volume) were prepared by adding 2 μL of 6 mg/mL

Table 1: Steady-State Kinetic Parameters for Fumarate Reduction in Wild-Type, H61M, and H61A Forms of Fcc_3 (25 °C and I = 0.50 M)

	k_{cat} (s^{-1})			K_m (μM)		
pH	wild-type[a]	H61M	H61A	wild-type[a]	H61M	H61A
6.0	658 ± 34	198 ± 7	116 ± 3	43 ± 10	9.9 ± 1.5	5.1 ± 0.7
7.2	509 ± 15	100 ± 3	49 ± 2	25 ± 2	5.0 ± 0.6	5.1 ± 0.6
7.5	370 ± 10	96 ± 3	47 ± 2	28 ± 3	4.9 ± 1.2	5.1 ± 0.7
9.0	210 ± 13	15 ± 2	29 ± 2	7 ± 2	0.7 ± 0.2	5.0 ± 0.2

[a] Values for the wild-type enzyme taken from ref *9*.

protein [in 10 mM Tris-HCl (pH 8.5)] to 2 μL of well solution. After approximately 10 days, needles of up to 1 mm × 0.2 mm × 0.2 mm and plates of up to 0.5 mm × 0.5 mm × 0.2 mm were formed. Crystals were immersed in a solution of 100 mM sodium acetate buffer (pH 6.5), 20% PEG 8000, 10 mM fumarate, and 80 mM NaCl, containing 23% glycerol as a cryoprotectant, prior to being mounted in nylon loops and flash-cooled in liquid nitrogen. For H61M-Fcc_3, a data set was collected to 2.1 Å resolution at beamline BW7A at DESY Hamburg (Hamburg, Germany) (λ = 0.9920 Å) using a Mar Research ccd detector, and for H61A Fcc_3, a data set was collected to 2.2 Å resolution at beamline BW7B at DESY Hamburg (λ = 0.8459 Å) using a Mar Research mar345 image plate detector. Crystals of both mutant forms belonged to space group $P2_1$. The H61M-Fcc_3 crystal had the following cell dimensions: a = 44.693 Å, b = 87.268 Å, c = 76.993 Å, and β = 104.353°. The H61A-Fcc_3 crystal had the following cell dimensions: a = 45.351 Å, b = 87.079 Å, c = 79.678 Å, and β = 109.381°.

Data processing was carried out using the HKL package (*26*). The wild-type Fcc_3 structure (1QJD), stripped of water, was used as the initial model for molecular replacement. Electron density fitting was carried out using the program Turbofrodo (*27*). Restraints for the FAD were calculated from two small molecule crystal structures (Cambridge Crystallographic Database entries HAMADPH and VEFHUJ10). Structure refinement was carried out using Refmac (*28*).

RESULTS

Molecular Mass and Flavin Content of Mutant Enzymes. The molecular masses of the mutant enzymes were determined by electrospray mass spectrometry (error ± 10 Da). In comparison to that of the wild type (63 033 Da), the mass difference was found to be −3 Da for H61M (expected difference of −6 Da) and −66 Da for H61A (expected difference of −66 Da). The average FAD content of the mutant enzymes was found to be 94 and 65% for H61M-Fcc_3 and H61A-Fcc_3, respectively. These compare with the typical value for the recombinant wild-type enzyme of ~73%. All catalytic rates were corrected for the variation in FAD content.

Steady-State Kinetics and Rescue of Activity. The ability of H61-substituted forms of Fcc_3 to catalyze fumarate reduction was determined under steady-state conditions over a range of pH values. The resulting k_{cat} and K_m parameters for wild-type and mutant forms of Fcc_3 are compared in Table 1. Both mutations result in a reduction in enzyme activity. At pH 7.2, for example, the k_{cat} values for the H61M and H61A mutant enzymes are 5- and 10-fold lower, respectively, than that seen for the wild-type enzyme. The

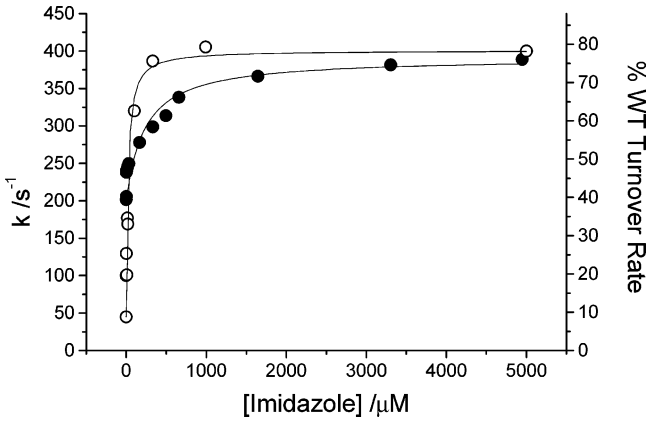

FIGURE 2: Effect of the addition of exogenous imidazole on fumarate reductase activity. Assays were performed under saturating substrate conditions (1 mM fumarate, 25 °C, pH 7.2, and I = 0.5 M). The concentration of imidazole in the assay was varied from 1 to 5000 μM. Actual turnover numbers are displayed on the left-hand axis, while the right-hand axis describes the turnover rate as a percentage of the maximal wild-type turnover rate observed (510 s^{-1}) in the absence of imidazole. Addition of imidazole to the wild-type Fcc_3 fumarate reductase assay gave no increase in the observed turnover rate. Empty and filled circles are for H61A and H61M, respectively.

K_m values for both mutant forms of Fcc_3 are also lower than that of the wild type. This means that, at pH 7.2, the k_{cat}/K_m (a measure of enzyme efficiency) value for the H61M enzyme is 2.0 × 10^7 M^{-1} s^{-1}, which is identical to that of the wild type within experimental error. At the same pH, the k_{cat}/K_m value for the H61A enzyme is half of that of the wild type at ~1.0 × 10^7 M^{-1} s^{-1}.

Full pH profiles of turnover rates, under substrate saturating conditions, give rise to pK_a values of 8.3 ± 0.2 and 9.3 ± 0.2 for H61A-Fcc_3 and H61M-Fcc_3, respectively. These values are significantly shifted from that of the wild type which is 7.5 ± 0.1 (*12*).

The fumarate activity of both the H61M and H61A mutant enzymes can be significantly rescued by addition of exogenous imidazole. Titration of the mutant enzymes with imidazole, under saturating turnover conditions, results in recovery of up to 80% of wild-type enzyme activity (Figure 2). The H61M and H61A mutant Fcc_3 enzymes display K_d values with imidazole of 230 ± 20 and 30 ± 6 μM, respectively. This difference can be explained by the larger steric bulk of the methionine side chain in the heme cavity of the H61M enzyme that would hinder the binding of imidazole and hence increase the K_d. It is very interesting to note that rescue of the activity of the H61A mutant enzyme, by exogenous imidazole, is accompanied by a shift in pK_a from 9.3 to 7.5 (Figure 3). This is close, and within experimental error, to the wild-type (WT) value. Titration of the enzyme with exogenous imidazole in the absence of substrate, however, yields dissociation constants for both the oxidized (K_d = 1.14 ± 0.08 μM) and reduced (K_d = 0.45 ± 0.06 μM) forms of H61A with the ligand that are 1 order of magnitude lower than those obtained in the presence of saturating substrate (Figure 4).

Solvent Isotope Effects. Proton inventories constructed for the WT and mutant forms of Fcc_3 all fit the model described by Schowen *et al.* (*24*) for multiple exchangeable hydrogenic sites in both reactant and transition states (Figure 5). Although mutations of His61 have not simplified the

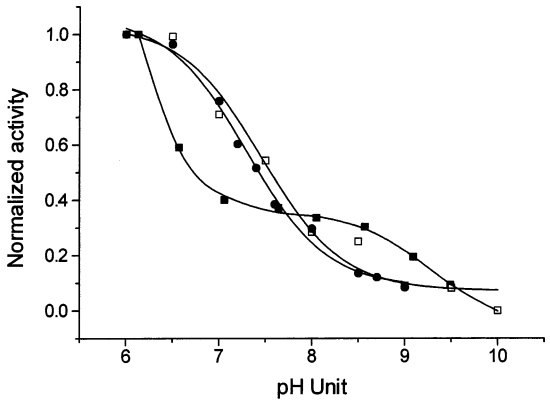

FIGURE 3: pH dependence of fumarate reductase activity under substrate saturating conditions (1 mM fumarate, 25 °C, and I = 0.5 M). Assays in the presence of imidazole were performed with a saturating (5 mM) imidazole concentration. The graph shows the normalized variation in turnover rate as a function of pH: wild type (●), H61A (■), and H61A with imidazole bound (□).

transition state, they have reduced the solvent kinetic isotope effect. Wild-type Fcc_3 displays a solvent kinetic isotope effect of 8.2 ± 0.4, whereas H61M and H61A have isotope effects of 5.6 ± 1.2 and 2.2 ± 0.9, respectively. Upon addition of saturating quantities of imidazole to the assay, the kinetic solvent isotope effect was seen to increase to 7.9 ± 1.3 and 8.1 ± 0.8 for the H61A and H61M mutant enzymes, respectively, i.e., back to the value seen for the wild-type enzyme.

Pre-Steady-State Kinetics. Stopped-flow analysis was used to monitor the course of fumarate-dependent heme oxidation at 418 nm. Data obtained for the recombinant wild-type enzyme were in good agreement with those obtained previously for the native enzyme, with the traces that were obtained fitting to a double-exponential curve (*19*). Rate constants of heme oxidation in the mutant forms of Fcc_3 are lower than with the wild-type enzyme (Table 2), but the decrease in k_{lim} is only 2-fold.

Potentiometric Titration. The reduction potentials of the four hemes in the mutant forms of Fcc_3 were investigated by potentiometric titrations. Results are shown in Figure 6, with the individual potentials given in Table 3. The titration curve for H61A-Fcc_3 is shifted by approximately 40 mV compared to that of the wild-type enzyme, whereas the more conservative H61M mutation displays a smaller shift of only approximately 25 mV. When repeated in the presence of saturating quantities of imidazole, the Nernst curves for both H61M- and H61A-Fcc_3 display a positive shift, and appear to converge toward a similar result.

Crystal Structures of the Mutant Flavocytochromes c_3. For the H61M and H61A mutant enzymes, data sets to resolutions of 2.1 and 2.2 Å, respectively, were used to refine the structures to final R-factors of 19.49% (H61M, R_{free} = 26.06%) and 17.51% (H61A, R_{free} = 25.81%) (Table 4). For each of the mutant enzymes, the model consists of one protein molecule comprising residues 1−568, four hemes, the FAD, one sodium ion, and a bound substrate molecule. In the case of the H61M enzyme, the molecule bound at the active site is the same malate-like species observed in the wild-type enzyme structure (*4*), whereas in the H61A enzyme, fumarate is bound at the active site in the same twisted conformation observed previously. In addition, the H61M model contains 581 water molecules and the H61A model 521 waters. At the C-terminus of the proteins, three residues (569−571) could not be located in the electron density maps. For both the H61A and H61M mutant enzymes, there is a small movement of the backbone between residues Thr49 and Ala/Met61 with respect to the wild-type structure. However, for all backbone atoms the rmsd fit is 0.3 Å between the H61M and wild-type enzymes and 0.4 Å between the H61A and wild-type enzymes, indicating no major differences between the protein structures.

In the structure of the H61M enzyme, it can be seen that the heme IV iron is coordinated by His86 on one side and by a water molecule (WAT578) on the other (Figure 7). In addition to the Fe-coordinating water molecule, WAT63 is 2.5 Å from WAT578 and WAT103 is 2.8 Å from WAT63, and these form an H-bonded "chain" above the heme plane. The residue introduced by the mutation, Met61, is seen to be oriented away from the heme at the surface of the protein, with the side chain sulfur atom H-bonded to two water molecules, WAT456 and WAT227. Interestingly, in this structure, the side chain of Ser60 is shown to be oriented over the heme plane, 3.3 Å from WAT578. In the structure of the H61A enzyme, the space vacated by substitution of His61 is occupied by an acetate ion presumably introduced as a result of the presence of 100 mM sodium acetate in the crystal cryoprotectant solution (Figure 7).

Substitution of His61 with either alanine or methionine is shown to make little difference in the relative positions of the cofactors of the enzyme, and in particular, the distance between heme IV and the FAD is shown to be 7.6 Å in the H61M enzyme and 7.7 Å in the H61A enzyme, compared to a value of 7.4 Å in the wild-type protein. In addition, substitution of His61 causes no structural changes at the active site, with the positions of putative proton transfer residues Glu378 and Arg381, and the active site acid catalyst (Arg402) remaining superimposable in all three structures (Figure 8).

DISCUSSION

Much of the recent work on Fcc_3 has focused on the flavin active site and the reduction of fumarate. On the basis of this work, a mechanism for fumarate reduction involving hydride transfer from FAD N5 and proton transfer from an arginine residue (Arg402) has become well-established (*4*, *9*−*14*, *29*). However, to understand this mechanism in a broader context, we must also consider how reducing equivalents are delivered to the FAD and the pathway by which protons reach the active site acid, Arg402. Analysis of the Fcc_3 crystal structure shows a clear route for electron transfer to FAD via the heme groups of the enzyme (Figure 1b). In addition, a proton delivery pathway involving Arg381, Glu378, and Arg402 has been identified (*9*, *11*, *13*, *14*).

In this report, we have focused on the delivery of electrons to the FAD via the heme groups. Although the route of electron transfer from membrane-bound quinols in *Shewanella* to Fcc_3 is not well-understood, recent studies have provided clear evidence that the physiological donor of an electron to Fcc_3 is the membrane-bound tetraheme cytochrome, CymA (*15*, *30*). It is likely that CymA donates electrons directly to one or more of the three solvent-exposed heme groups (I−III) of Fcc_3 (Figure 1a). Protein film voltammetry studies have led to the suggestion that this chain of heme groups might function predominantly by simply

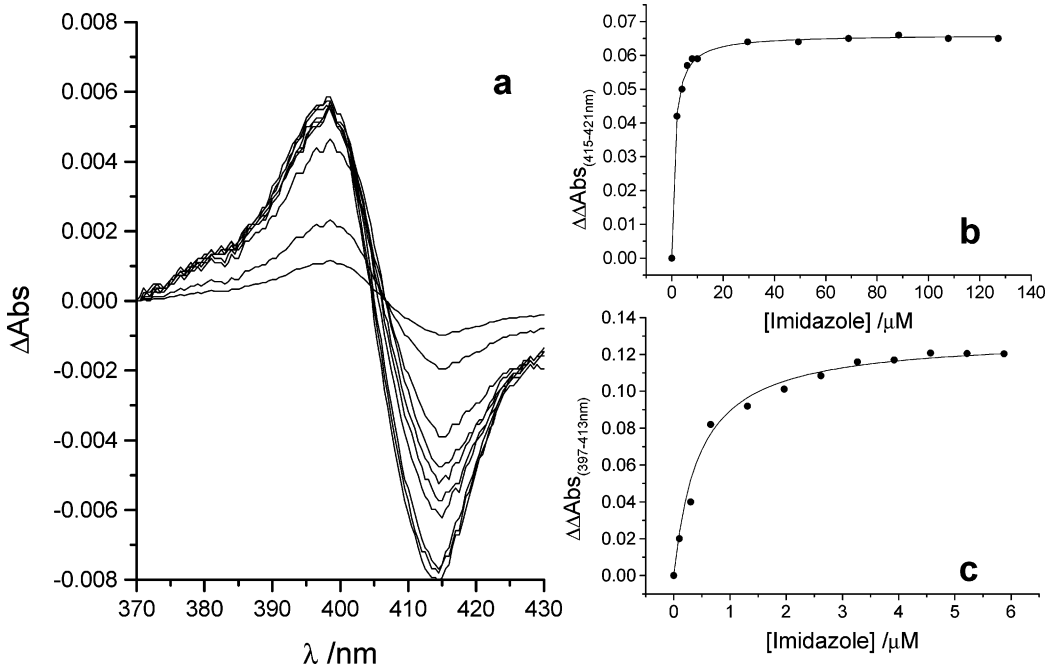

FIGURE 4: Addition of increasing concentrations of imidazole to the H61A-Fcc_3 enzyme. All experiments were performed at 25 °C, pH 7.2, and an ionic strength of 0.5 M. (a) The difference spectra were generated by subtraction of the spectra for the ligand-bound form of the oxidized enzyme from the spectra for the ligand free form of the oxidized enzyme. The same procedure was employed for determining dissocation constants for ligand binding to the reduced form of the enzyme (data not shown). (b) The relationship between the maximum absorbance change and ligand concentration from the data given in panel a gives a K_d for binding to the oxidized enzyme of 0.45 ± 0.06 μM. (c) The relationship between the maximum absorbance change and the concentration of the ligand when bound to the reduced form of the H61A-Fcc_3 enzyme gives a K_d for imidazole binding of 1.14 ± 0.08 μM. Ligand dissociation constants for exogenous imidazole binding to both oxidized (b) and reduced (c) forms of the enzyme were evaluated via fitting to a hyperbolic function.

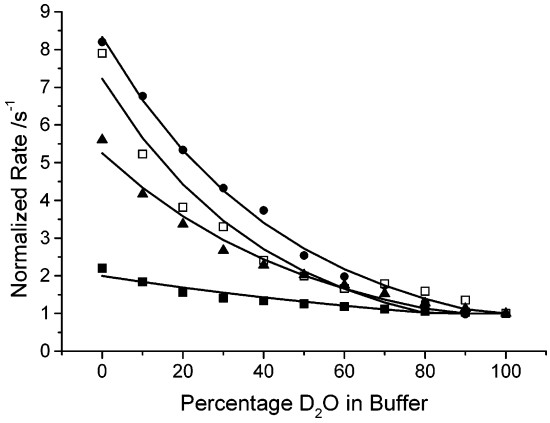

FIGURE 5: Effect on the observed turnover rate upon partial deueration of the assay buffer. All assays were carried out at 25 °C, pL 7.2, and an ionic strength of 0.5 M and under saturating fumarate concentrations (1 mM). All data sets are fitted to a multisite model as discussed in the text. The left-hand axis has been normalized according to the overall kinetic solvent isotope effect displayed by the enzyme: (●) WT, (▲) H61M, (■) H61A, and (□) H61A and imidazole.

increasing the electronic coupling between the donor (in this case CymA) and the FAD (*31*). In this respect, and in light of the structure, it is conceivable that electron transfer to the FAD might not need to involve all four heme groups. What is clear, however, is that electron transfer to the FAD must occur via heme IV, because this heme is buried within the protein and adjacent to the FAD (Figure 1). One of the histidine ligands to heme IV (His61) is only 8.4 Å from the FAD.

The substitution of His61 in Fcc_3 with either methionine or alanine leads to mutant enzymes that have reduced catalytic activity for fumarate reduction (Table 1). At pH 7.2, the k_{cat} value for the H61M enzyme is ~5-fold lower than that of the wild type, and for H61A, it is ~10-fold lower. Interestingly, there is a similar trend in the K_m values, which means that the catalytic efficiencies of the mutant enzymes (as judged by k_{cat}/K_m) are very similar to that of the wild-type enzyme. This correlation of K_m with k_{cat} is consistent with a change in the rate-determining step in the catalytic cycle. This idea is given support by the dependence of fumarate reductase activity on pH, which has been significantly altered by the mutations. The pK_a seen in the activity profile for the wild-type enzyme is 7.5 ± 0.1, and this value has been assigned to an active site histidine, His504 (*10*, *12*). In the mutant enzymes, the pK_a value has been shifted to 8.3 ± 0.2 and 9.3 ± 0.2 for H61M and H61A, respectively. An examination of the X-ray crystal structures of the three forms of Fcc_3 (Figure 8) shows an overlay of the active site in the wild-type, H61M, and H61A enzymes. It can clearly be seen that all of the catalytically essential residues, including His504, are virtually superimposable. It is therefore unlikely that the shifts in the pK_a value are due to perturbations of His504. The most likely explanation for such changes in pK_a is that an alternative ionizable group, associated with a new transition state, is being deprotonated or protonated. The question is whether the rate-determining step has been changed and if so what limits the rate of the catalytic cycle in the mutant enzymes.

For the wild-type enzyme, it has previously been shown that electron transfer through the hemes to the FAD is fast and cannot be rate-limiting (*16*). It was suggested that the main rate limitation to catalytic turnover is proton delivery (*16*, *19*). Support for this suggestion has come from proton

Table 2: Pre-Steady-State Kinetic Parameters for Fumarate-Dependent Heme Reoxidation in Wild-Type, H61M, and H61A Forms of Fcc_3 (25 °C, pH 7.2, and $I = 0.50$ M)

	k_{lim} (s^{-1})			K (μM)		
	wild-type[a]	H61M	H61A	wild-type[a]	H61M	H61A
fast phase	420 ± 16	210 ± 9	162 ± 10	23 ± 3	24 ± 4	10.2 ± 1.5
slow phase	68 ± 5	42 ± 5	23 ± 3	33 ± 3	36 ± 10	54 ± 19

[a] Values for the wild-type enzyme taken from ref *9*.

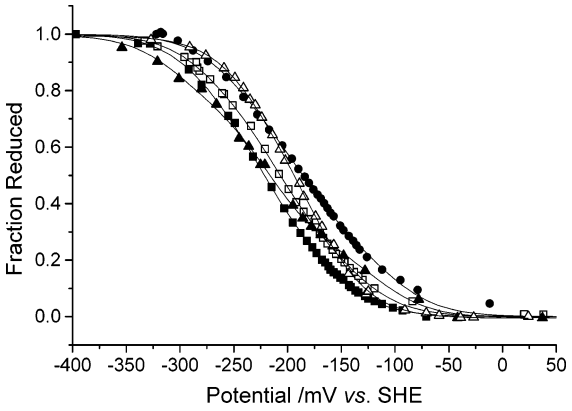

FIGURE 6: Potentiometric titration of wild-type (●), H61M (▲), and H61A (■) Fcc_3. Titrations in the presence of 5 mM imidazole of the H61M and H61A mutants are shown with empty triangles and squares, respectively. The graph shows the extent of heme reduction of the tetraheme moiety, monitored at 552 nm as a function of the reduction potential. Data were recorded at 25 °C, pH = 7.0, and an ionic strength of 0.1 M, and fitted as described in the text, using the equation described previously (*22*).

Table 3: Formal Reduction Potentials (millivolts vs the SHE) of Wild-Type, H61M, and H61A Forms of Fcc_3 Determined from Reductive and Oxidative Potentiometric Titrations (25 °C, pH 7.0, and $I = 0.1$ M)[a]

	wild-type[b]	H61M	H61M and imidazole[c]	H61A	H61A and imidazole[c]
E_1	−126	−128	−144	−158	−137
E_2	−182	−198	−208	−221	−193
E_3	−225	−208	−217	−236	−227
E_4	−295	−268	−270	−270	−262

[a] E_1−E_4 are the potentials of the four successive one-electron reductions of the tetraheme moiety. [b] Values for wild type have been redetermined, and supersede those reported in ref *22*. [c] In the presence of 5 mM imidazole.

inventory and solvent kinetic isotope effect (SKIE), studies. The proton inventory for wild-type Fcc_3 (Figure 5) fits to a model for multiple exchangeable sites in both transition and reactant (Michaelis complex) states (*24*). Such a fit is consistent with (but does not prove) the idea of a proton pathway involving a number of exchangeable sites as previously proposed (*9*, *11*, *13*−*15*). In addition, at pL 7.2, wild-type Fcc_3 has a large SKIE value (k_H/k_D) of 8.2 ± 0.4. These results taken together are consistent with a mechanism in which proton delivery to the substrate is the major rate-determining step for catalysis in the wild-type enzyme. However, SKIE values for the mutant enzymes are substantially lower than that seen for the wild type, falling to 5.6 ± 1.2 for H61M-Fcc_3 and to 2.2 ± 0.9 for H61A-Fcc_3. These substantial decreases in SKIE indicate that proton delivery is becoming less rate-limiting in the mutant enzymes. In fact, in the case of the H61A mutant enzyme, proton delivery exerts very little control on the rate of catalysis.

Table 4: Data Collection and Refinement Statistics

	H61M	H61A
resolution (Å)	17.0−2.1	17.0−2.2
total no. of reflections	283176	205404
no. of unique reflections	32878	29268
completeness (%)	98.3	98.4
$I/\sigma(I)$	18.4	10.6
R_{merge} (%)[a]	6.1	7.4
R_{merge} in the outer shell (%)	25.3 (2.17−2.10 Å)	28.6 (2.28−2.20 Å)
R_{cryst} (%)[b]	19.49	17.51
R_{free} (%)[b]	26.06	25.81
rmsd from ideal values		
bond lengths (Å)	0.018	0.016
bond angles (deg)	3.7	3.4
Ramachandran analysis		
most favored (%)	86.5	87.9
additionally allowed (%)	13.3	11.9

[a] $R_{merge} = \sum_h\sum_i|I(h) - I_i(h)|/\sum_h\sum_i I_i(h)$, where $I_i(h)$ and $I(h)$ are the ith and mean measurements of reflection h, respectively. [b] $R_{cryst} = \sum_h|F_o - F_c|/\sum_h F_o$, where F_o and F_c are the observed and calculated structure factor amplitudes of reflection h, respectively. R_{free} is the test reflection data set, 5% selected randomly for cross validation during crystallographic refinement.

It would appear then that changes in heme IV caused by the mutations have slowed electron delivery to the FAD. Thus, electron transfer to the FAD, and not proton transfer, becomes more rate-limiting, and hence, the SKIE values are much smaller in the mutant enzymes. One possible reason for the reduction of the electron transfer rate is that the mutations have introduced significant reorganization energies at heme IV.

The impairment of electron transfer is also reflected in the pre-steady-state analysis of the mutant enzymes (Table 2). The stopped-flow data are complex and do not represent a simple microscopic rate constant. It has been previously shown that fumarate-dependent oxidation of the heme groups in wild-type Fcc_3 gives rise to biphasic traces (*19*). This arises because fully reduced Fcc_3 is loaded with six electrons (two on the flavin and one on each of the four hemes). Thus, the two-electron reduction of three fumarate molecules is required to fully oxidize Fcc_3. Heme oxidation monitored at 418 nm results in biphasic traces with each phase corresponding to half the total absorbance change. Each of these phases has been previously assigned to the oxidation of two of the four hemes, and it has been suggested that the hemes may be functionally paired to facilitate the delivery of two electrons to the FAD and hence to the substrate (*19*). This biphasic behavior is also observed in both mutant enzymes. However, values of k_{lim} for both fast and slow phases are lower than that seen for the wild type (Table 2). The trend is similar to that seen for k_{cat} with the H61A enzyme being more affected than the H61M enzyme.

If electron transfer really has become rate-limiting, and this is due to the loss of the His61 ligand, then we reasoned that it might be possible to recover some of the original

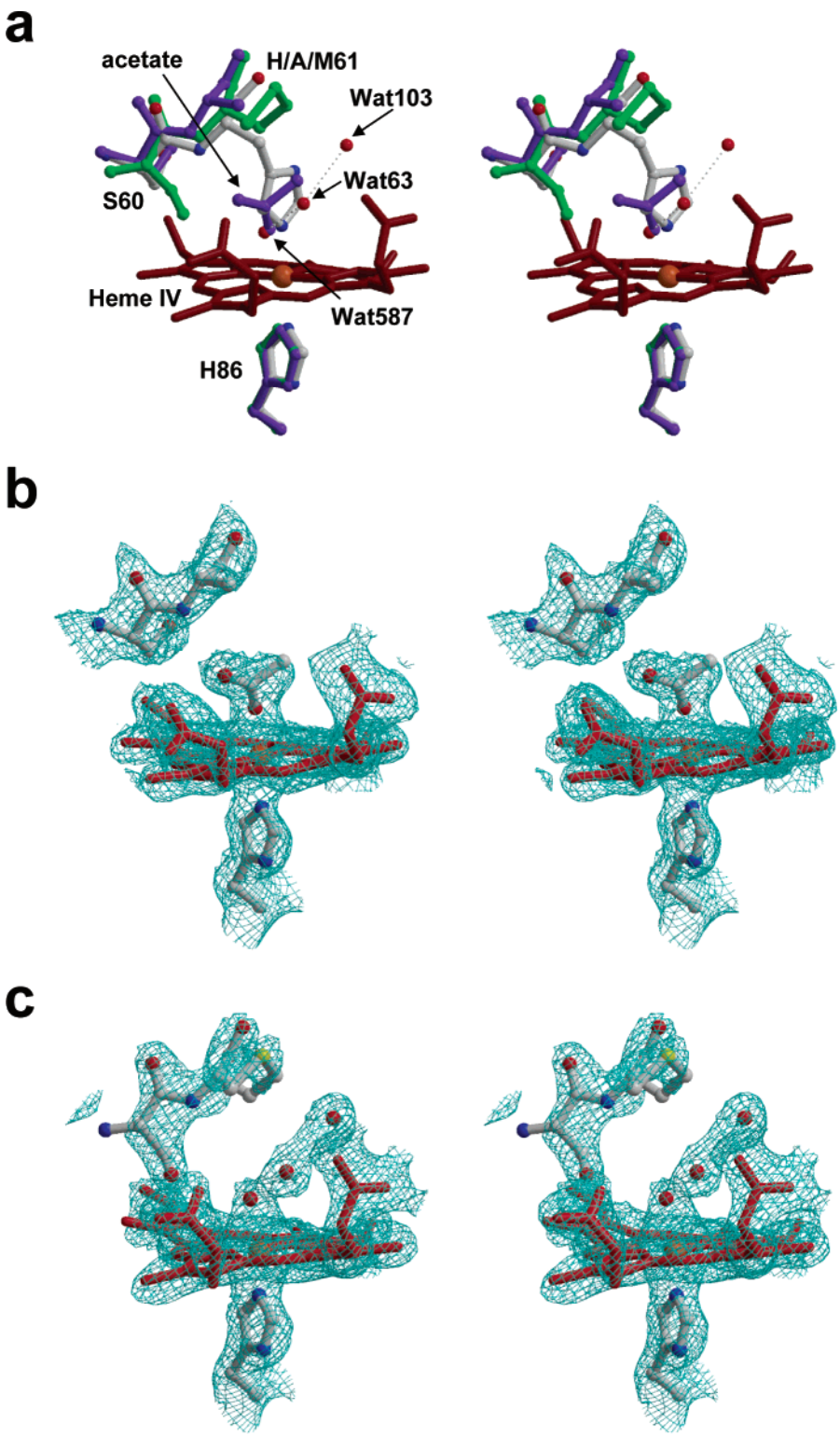

FIGURE 7: (a) Stereo-overlay of the region around heme IV in wild-type (gray), H61M (green), and H61A (purple) flavocytochromes c_3. For clarity, heme IV is shown for only the wild-type enzyme. Panels b and c show stereoviews of the electron density around heme IV in the H61A and H61M mutant enzymes, respectively. Electron density maps were calculated using Fourier coefficients $2F_o - F_c$, where F_o and F_c are the observed and calculated structure factors, respectively, the latter based on the final model. The contour level is 1σ, where σ is the rms electron density. This figure was generated using BOBSCRIPT (*33*) and RASTER3D (*34*).

activity by the addition of imidazole to the mutant enzymes. This proved to be the case. Addition of imidazole to the H61A and H61M enzymes under turnover conditions resulted in recovery of ~80% of the activity seen for the wild-type enzyme (Figure 2). In addition, it was observed that for the H61A mutant enzyme the recovery of activity was accompanied by a shift in pK_a from 9.3 to the wild-type value of 7.5. Imidazole-induced recovery of activity in the H61A mutant also resulted in the SKIE value increasing from 2.2 ± 0.9 to 7.9 ± 1.3, close to the value for the wild-type enzyme.

It is apparent from ligand binding studies that imidazole binds much tighter to the H61A enzyme than to the H61M enzyme. This can be explained very easily by an examination

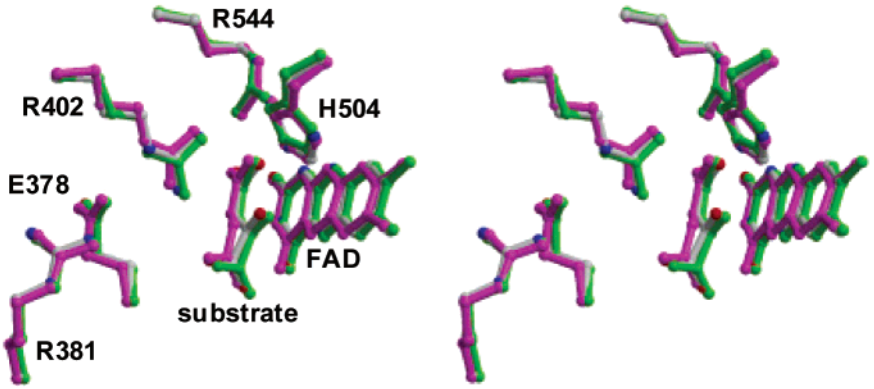

FIGURE 8: Stereo-overlay of the active sites of the wild-type (gray), H61A (magenta), and H61M (green) flavocytochromes c_3. From this figure, it can be clearly seen that there is no change in the position of any of the important active site residues as a result of either mutation. This figure was generated using BOBSCRIPT (*33*) and RASTER3D (*34*).

of the environment around heme IV (Figure 7). In the structure of the H61A mutant enzyme, it is clear that, in the absence of the histidine side chain (and also of the introduced acetate molecule seen in the structure), there is an ideal cavity available to accommodate the imidazole group. However, in the H61M structure, even though the methionine is clearly not ligating the iron, the steric bulk of the side chain makes it difficult for the imidazole to bind, leading to the much higher K_d value seen with this mutant. In the structure of the H61M mutant enzyme, it is perhaps reasonable to expect that introduction of Met61 would lead to His−Met coordination of the heme IV iron, as is seen in cytochrome *c*. Evidently, this is not the case, and the iron is ligated by a water molecule. For Met61 to ligate the heme iron, there would need to be a movement of the protein backbone in the region of residue 61 toward the heme group. This, however, does not occur. The actual position taken by the side chain of Met61 is at the surface of the protein, exposed to solvent and clearly quite mobile as evidenced by relatively high *B*-factors for the side chain atoms. The other interesting difference at heme IV in the H61M mutant enzyme is the position of the side chain of Ser60 over the heme plane. The reason for this conformational change is not totally clear. It is possible that it arises because of the subtle changes in the protein backbone as a result of the mutation, or that there is an interaction with the iron-ligating water molecule (WAT578), although such a hydrogen bonding interaction would be weak given the long distance between the serine hydroxyl group and the water molecule (3.3 Å).

One possibility that must be considered when altering the ligation around a heme iron is that there may be a substantial effect on the reduction potential. To examine this, we carried out potentiometric titrations on both mutant enzymes. These titrations indicate only minor differences between the Nernst curves for the wild-type enzyme and the two mutants (Figure 6). The effects on individual heme reduction potentials are complex, and given that the error values are at least ±10 mV, it is difficult to make any definitive statements apart from the fact that the changes are too small to have a significant effect on the turnover of the enzyme.

Consequently, the imidazole ring of His61 appears to be important in controlling the passage of reducing equivalents from the heme chain to the FAD and, as a direct result, plays a vital role in the control of fumarate reduction.

ACKNOWLEDGMENT

We thank Dr. Myles Cheesman, Prof. Carlos Salgueiro, and Miguel Pessanha for helpful discussions.

REFERENCES

1. Iverson, T. M., Luna-Chavez, C., Cecchini, G., and Rees, D. C. (1999) *Science 284*, 1961−1966.
2. Körtner, C., Lauterbach, F., Tripier, D., Unden, G., and Kröger, A. (1990) *Mol. Microbiol. 4*, 855−860.
3. Gordon, E. H. J., Pealing, S. L., Chapman, S. K., Ward, F. B., and Reid, G. A. (1998) *Microbiology 4*, 937−945.
4. Taylor, P., Pealing, S. L., Reid, G. A., Chapman, S. K., and Walkinshaw, M. D. (1999) *Nat. Struct. Biol. 6*, 1108−1112.
5. Leys, D., Tsapin, A. S., Nealson, K. H., Meyer, T. E., Cusanovich, M. A., and Van Beeumen, J. J. (1999) *Nat. Struct. Biol. 6*, 1113−1117.
6. Bamford, V., Dobbin, P. S., Richardson, D. J., and Hemmings, A. M. (1999) *Nat. Struct. Biol. 6*, 1104−1107.
7. Lancaster, C. R. D., Kröger, A., Auer, M., and Michel, H. (1999) *Nature 402*, 377−385.
8. Lancaster, C. R. D., Gross, R., and Simon, J. (2001) *Eur. J. Biochem. 268*, 1820−1827.
9. Doherty, M. K., Pealing, S. L., Miles, C. S., Moysey, R., Taylor, P., Walkinshaw, M. D., Reid, G. A., and Chapman, S. K. (2000) *Biochemistry 39*, 10695−10701.
10. Reid, G. A., Miles, C. S., Moysey, R. K., Pankhurst, K. L., and Chapman, S. K. (2000) *Biochim. Biophys. Acta 1459*, 310−315.
11. Mowat, C. G., Moysey, R., Miles, C. S., Leys, D., Doherty, M. K., Taylor, P., Walkinshaw, M. D., Reid, G. A., and Chapman, S. K. (2001) *Biochemistry 40*, 12292−12298.
12. Pankhurst, K. L., Mowat, C. G., Miles, C. S., Leys, D., Walkinshaw, M. D., Reid, G. A., and Chapman, S. K. (2002) *Biochemistry 41*, 8551−8556.
13. Mowat, C. G., Pankhurst, K. L., Miles, C. S., Leys, D., Walkinshaw, M. D., Reid, G. A., and Chapman, S. K. (2002) *Biochemistry 41*, 11990−11996.
14. Chapman, S. K., Morrison, C. A., Reid, G. A., Pealing, S. L., Taylor, P., and Walkinshaw, M. D. (1999) in *Flavins and Flavoproteins 1999* (Ghisla, S., Kroneck, P., Macheroux, P., and Sund, H., Eds.) pp 105−113, Rudolf Weber, Agency for Scientific Publications, Berlin.
15. Schwalb, C., Chapman, S. K., and Reid, G. A. (2002) *Biochem. Soc. Trans. 30*, 658−662.
16. Jones, A. K., Camba, R., Reid, G. A., Chapman, S. K., and Armstrong, F. A. (2000) *J. Am. Chem. Soc. 122*, 6494−6495.
17. Kunkel, T. A., and Roberts, J. D. (1987) *Methods Enzymol. 154*, 367−382.
18. Michel, L. O., Sandkvist, M., and Bagdasarian, M. (1995) *Gene 152*, 41−45.
19. Pealing, S. L., Cheesman, M. R., Reid, G. A., Thomson, A. J., Ward, F. B., and Chapman, S. K. (1995) *Biochemistry 34*, 6153−6158.

20. Pealing, S. L., Lysek, D. A., Taylor, P., Alexeev, D., Reid, G. A., Chapman, S. K., and Walkinshaw, M. D. (1999*) J. Struct. Biol. 127*, 76−78.
21. Macheroux, P. (1999) in *Flavoprotein Protocols: Methods in Molecular Biology* (Chapman, S. K., and Reid, G. A., Eds.) Vol. 131, pp 1−7, Humana Press, Totowa, NJ.
22. Turner, K. L., Doherty, M. K., Heering, H. A., Armstrong, F. A., Reid, G. A., and Chapman, S. K. (1999) *Biochemistry 38*, 3302−3309.
23. Glascoe, P. K., and Long, F. A. (1960) *J. Phys. Chem. 64*, 188−191.
24. Schowen, K. B., and Schowen, R. L. (1982) *Methods Enzymol. 87*, 551−606.
25. Dutton, P. L. (1978) *Methods Enzymol. 54*, 411−435.
26. Otwinowski, Z., and Minor, W. (1997) *Methods Enzymol. 276*, 307−326.
27. Roussel, A., and Cambillau, C. (1991) TURBO-FRODO, in *Silicon Graphics Geometry Partners Directory 86*, Silicon Graphics, Mountain View, CA.
28. Murshudov, G. N., Vagin, A. A., and Dodson, E. J. (1997) *Acta Crystallogr. D53*, 240−255.
29. Mowat, C. G., Miles, C. S., Reid, G. A., Walkinshaw, M. D., Pankhurst, K. L., Chapman, S. K., and Leys, D. (2002) in *Flavins and Flavoproteins 2002* (Chapman, S. K., Perham, R., and Scrutton, N., Eds.) pp 739−748, Rudolf Weber, Agency for Scientific Publications, Berlin.
30. Schwalb, C., Chapman, S. K., and Reid, G. A. (2003) *Biochemistry 42*, 9491−9497.
31. Jeuken, L. J. C., Jones, A. K., Chapman, S. K., Cecchini, G., and Armstrong, F. (2002) *J. Am. Chem. Soc. 124*, 5702−5713.
32. Pankhurst, K. L., Rothery, E. L., Doherty, M. K., Chapman, S. K., Mowat, C. G., Miles, C. S., and Reid, G. A. (2002) in *Flavins and Flavoproteins 2002* (Chapman, S. K., Perham, R., and Scrutton, N., Eds.) pp 779−784, Rudolf Weber, Agency for Scientific Publications, Berlin.
33. Esnouf, R. M. (1997) *J. Mol. Graphics 15*, 132−134.
34. Merritt, E. A., and Murphy, M. E. P. (1994) *Acta Crystallogr. D50*, 869−873.

BI030159Z